Sensors and Materials, Vol. 34, No. 5 (2022) 1991–1999
MYU Tokyo

S & M 2948

Visible-light Photocatalytic Study of SnOx:N Islands on Bi_2MoO_6

Wan-Chun Yang,[1] David Jui-Yang Feng,[1] Hsin-Hui Kuo,[1] Ming-Chang Shih,[1]
Mu-Chun Wang,[2] Chien-Jung Huang,[3] and Wen-How Lan[1*]

[1]Department of Electrical Engineering, National University of Kaohsiung,
700, Kaohsiung University Rd., Nanzih District, Kaohsiung 81148, Taiwan, R.O.C.
[2]Department of Electronic Engineering, Minghsin University of Science and Technology,
No. 1, Xinxing Rd., Xinfeng Hsinchu 30401, Taiwan, R.O.C.
[3]Department of Applied Physics, National University of Kaohsiung,
700, Kaohsiung University Rd., Nanzih District, Kaohsiung 81148, Taiwan, R.O.C.

(Received November 28, 2021; accepted April 14, 2022)

Keywords: visible-light photocatalytic, Bi_2MoO_6, islanding SnOx:N

Developing a visible-light (VL) photocatalytic composite to decompose organic pollutants is a major challenge in environmental protection. Toward the photocatalytic application of the sensor material Bi_2MoO_6, a novel structure containing SnOx:N islands was constructed by co-spraying SnOx:N/ZnO species on a sprayed Bi_2MoO_6 surface, which was followed by ZnO etching with buffered HF. The effects of the etching time on the surface morphology and composite were studied. The photocatalytic ability of the composite was evaluated on the degradation of RhB under VL LED illumination. For a sample subjected to 30 s etching with exposed Bi_2MoO_6 and SnOx:N islands on the surface, relatively high photocatalytic activity with a reaction rate constant of 0.0124 min^{-1} was obtained. On the basis of the scavenger analysis of the composites, the photocatalytic mechanism and the effect of etching were discussed.

1. Introduction

Aurivillius-type materials have attracted considerable interest in recent years. Among them, bismuth molybdate (Bi_2MoO_6), which is constructed from layered bismuth oxide $Bi_2O_2^{2+}$ with perovskite octahedral MoO_4^{2-}, shows excellent performance in humidity,(1) nitrogen oxide,(2) and ethanol(3) sensing. Because of its high capacity to adsorb chemicals in its sandwiched layer structure, adsorbed species can be further decomposed under light excitation. In addition to its sensing ability, Bi_2MoO_6 also shows promising catalytic ability under light irradiation. For the benchmark photocatalytic material TiO_2, UV light illumination is necessary for electron and hole generation due to its wide bandgap of 3.2 eV.(4) Because the visible light (VL) energy in the solar spectrum is greater than that of UV light, shifting the operating spectrum to the VL band has become one of the hot strategies for developing photocatalysts. Bi_2MoO_6 shows the just-matched status because its bandgap is around 2.6 eV(5) with electron and hole generation under VL illumination. The promising photocatalytic ability of Bi_2MoO_6 for the degradation of RhB under VL illumination has been reported.(6)

*Corresponding author: e-mail: whlan@nuk.edu.tw
https://doi.org/10.18494/SAM3752

ISSN 0914-4935 © MYU K.K.

To further increase photocatalytic ability, heterocomposites have been developed. Bi_2MoO_6-related heterostructures such as $Bi_2MoO_6/ZnIn_2S$[7] and Bi_2MoO_6/SnO_2[8] have shown promising photocatalytic ability due to enhanced light absorption, reduced internal recombination, and efficient carrier separation for their reaction.

Bi_2MoO_6 can be fabricated by many techniques such as thermal evaporation,[9] the Teflon-lined autoclave method,[10] and the co-precipitation method.[11] Spray pyrolysis is a promising method for large-area fabrication. In our previous study, a heterostructure comprising SnOx:N on a Bi_2MoO_6/MoO_3 composite prepared by spray pyrolysis showed enhanced photocatalytic activity upon N doping owing to its increased conductivity.[12]

In a photocatalyst, photon-excited electrons and holes are separated and transported to the surface to undergo a photoreaction. For a catalyst with multiple compositions operating in VL, the Z-scheme[13] is generally considered to occur. In this scheme, high-energy electrons and holes are transported to different surfaces. The electrons, holes, and radicals generated by the electrons and holes undergo a degradation reaction. The exposed surfaces for the electron-dominated and hole-dominated reactions thus have the main effect on the degradation reaction in the Z-scheme. It is known that the surface condition[14] affects the photocatalytic ability. However, there has been less study on the controlled electron-dominated and hole-dominated surfaces for the photocatalytic reactions in the Z-scheme. In this paper, we propose a novel catalyst structure of SnOx:N islands on Bi_2MoO_6 with a controlled SnOx:N surface for the hole-dominated reaction and a Bi_2MoO_6 surface for the electron-dominated reaction. The structure was formed by co-spraying SnOx:N/ZnO on Bi_2MoO_6 followed by ZnO etching. The effects of the etching time on the morphology and photocatalytic ability of the films for the degradation of RhB under VL illumination were investigated.

2. Experimental Methods

In this work, all composites were deposited on an n-type Si (111) substrate with resistivity 1–5 Ω·cm by spray pyrolysis. The Si substrate was cut to 2.5 cm × 2.5 cm, cleaned using isopropanol (IPA), acetone, DI water, and buffered HF (BHF); rinsed with DI water; and dried in nitrogen (N_2) gas. Bi_2MoO_6 was deposited at 450 °C using ammonium molybdate [$(NH_4)_6Mo_7O_{24}{\cdot}4H_2O$, 0.2 M] and bismuth(III) nitrate pentahydrate [$Bi(NO_3)_3{\cdot}5H_2O$, 0.01 M] precursors, with a thin ZnO underlayer deposited using a zinc acetate [$Zn(CH_3COO)_2{\cdot}2H_2O$, 0.2 M] precursor to ensure film adhesion. The thicknesses of ZnO and Bi_2MoO_6 were around 40 and 200 nm, respectively. The temperature was decreased to 300 °C and ZnO and SnOx:N were co-sprayed from two precursor sources containing zinc acetate (0.2 M), and mixed stannous chloride ($SnCl_2$, 0.1 M) and ammonium acetate (CH_3COONH_4, N/Sn = 25%) aqueous solution, respectively. After deposition, the film was dipped in BHF to form SnOx:N islands. Samples are denoted as BS*x*, where *x* represents the dip time in seconds. For example, BS30 refers to the Bi_2MoO_6/(SnOx:N,ZnO) sample dipped in BHF in 30 s then rinsed in DI water and dried in N_2 gas. The height of the SnOx:N islands was around 330 nm. A sample containing SnOx:N on Bi_2MoO_6 without co-sprayed ZnO was also prepared by the same procedure, which is denoted as BS. In addition, Bi_2MoO_6 with a ZnO underlayer on Si (denoted as ZB) and SnOx:N on Si

(denoted as SS) were deposited with the above deposition parameters for XRD measurement and BHF etching analysis, respectively. ZnO was also deposited on Si at 300 ºC with the same deposition parameters as above for BHF etching analysis.

In the photocatalytic study, 10 mL of RhB aqueous solution with an initial concentration of 10 ppm was used with a 14 W VL LED bulb (Philips). The relative RhB concentration was determined by colorimetry. The crystallinity was characterized by X-ray diffraction (XRD) analysis (Bruker D8, Billerica, MA, USA). The surface morphology was examined by scanning electron microscopy (SEM, Hitachi S-4300N, Tokyo, Japan).

3. Results and Discussion

Figures 1(a) and 1(b) respectively show the XRD patterns of samples ZB and SS. For sample ZB, peaks corresponding to Bi_2MoO_6 (JCPDS 21-0102)[15] and ZnO (89-1397)[16] groups can be distinguished. No MoO_3- or Bi_2O_3-related signals were found. Thus, the structure of the underlying ZnO is not affected by the following Bi_2MoO_6 deposition at 450 ℃. For sample SS, the peaks correspond to Sn_3O_4 (JCPDS 16-0737) and tetragonal SnO_2 (JCPDS 41-1445).[17] Thus, the SnOx:N contains a mixed structure of SnO_2 and Sn_3O_4.

Figure 2 shows SEM images of samples (a) BS, (b) BS0, (c) BS10, (d) BS30, and (e) BS90. For BS, the sample with SnOx:N on the surface, a textured surface with some spherical granules on it was observed. For BS0, the sample with mixed SnOx:N/ZnO on the surface, a uniform grain morphology was observed. For BS10, spherical particles with a diameter of around 150–400 nm were observed. The etching rates of the deposited ZnO film, SnOx:N film, and Bi_2MoO_6 film in BHF were more than 15 nm/s, less than 0.1 nm/s, and 0.5 nm/s, respectively. The SnOx:N was BHF-resistant, whereas ZnO was etched easily with BHF. SnOx:N spherical granules remained on the surface of BS10. For BS30, a similar morphology to BS10 but with fewer spherical granules was observed. Although the SnOx:N could resist BHF etching, some of the SnOx:N composite may have been lifted off by BHF along with the ZnO beneath. For BS90, more of the SnOx:N composite was lifted off and fewer spherical granules were observed.

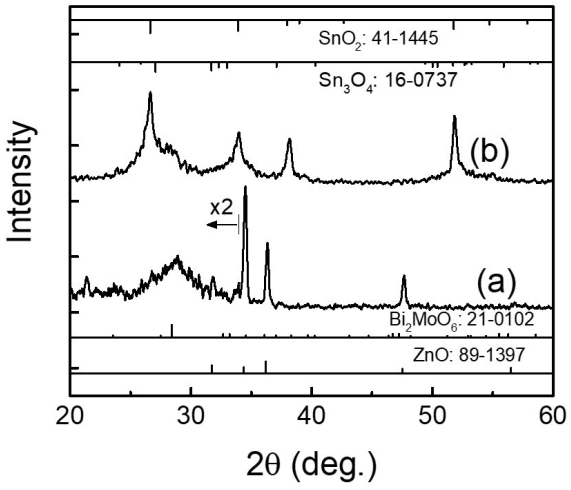

Fig. 1. XRD patterns of samples (a) ZB and (b) SS.

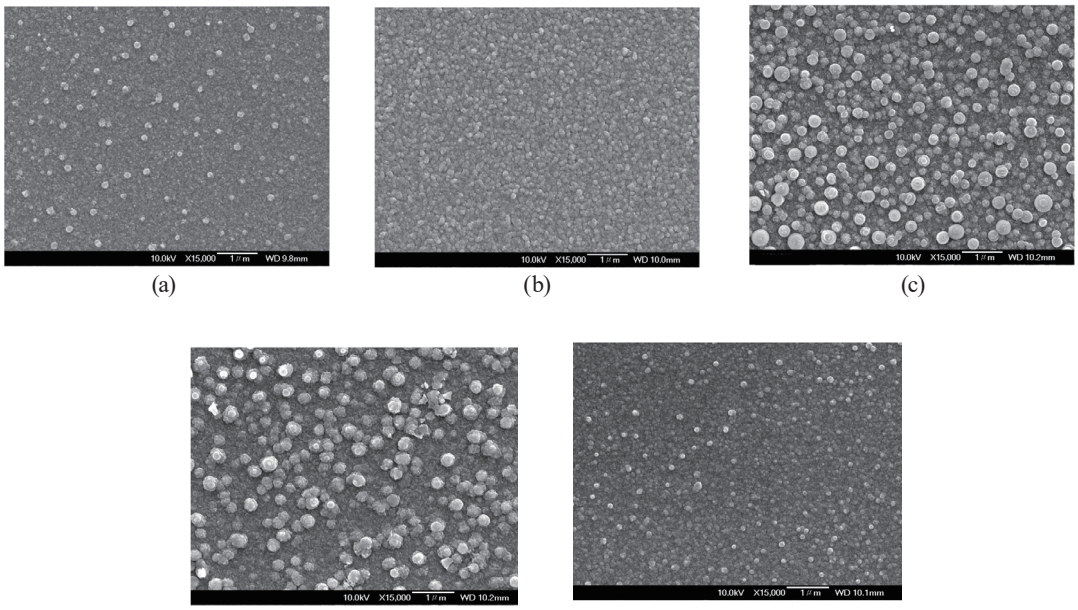

(a) (b) (c) (d) (e)

Fig. 2. SEM images of samples (a) BS, (b) BS0, (c) BS10, (d) BS30, and (e) BS90.

Figures 3(a)–3(d) respectively show the energy-dispersive X-ray spectroscopy (EDS) spectra of BS, BS0, BS30, and BS90, and Fig. 3(e) shows the relative count ratio of Zn to Sn ($CR_{Zn/Sn}$) for these samples. For BS0, $CR_{Zn/Sn}$ is higher than that of BS due to the introduced ZnO mixed with SnOx:N on the surface. For BS30, because the ZnO surface is etched by BHF, $CR_{Zn/Sn}$ is reduced to a value near that of BS. For BS90, $CR_{Zn/Sn}$ is higher than that of BS30. Although the etching rate of SnOx:N in BHF is smaller than that of ZnO, a small amount of SnOx:N was etched and some of the N:SnOx composite may have lifted off along with the mixed ZnO beneath for the sample immersed in BHF for 90 s. This caused the increase in $CR_{Zn/Sn}$ for BS90 compared with that for BS30.

The degradation efficiency D in our photocatalytic analysis is defined as[18]

$$D\,(\%) = (1 - C / C_0) \times 100\%, \tag{1}$$

where C_0 is the RhB concentration at equilibrium adsorption and C is the residual concentration of RhB at illumination time t. The degradation efficiency D of RhB for BS, BS0, BS10, BS30, BS60, and BS90 samples under VL LED illumination is shown in Fig. 4(a). Relatively high degradation efficiency for sample BS can be seen. The photodegradation reaction of RhB was based on pseudo-first-order kinetics with the formula[19]

$$-\ln (C / C_0) = k \cdot t, \tag{2}$$

where k is the reaction rate constant. The values of k for these samples are shown in Fig. 4(b). For sample BS, a reaction occurred on the surface under VL illumination. For sample BS0, with mixed SnOx:N/ZnO on the surface, the reaction was inhibited by ZnO covering the surface and

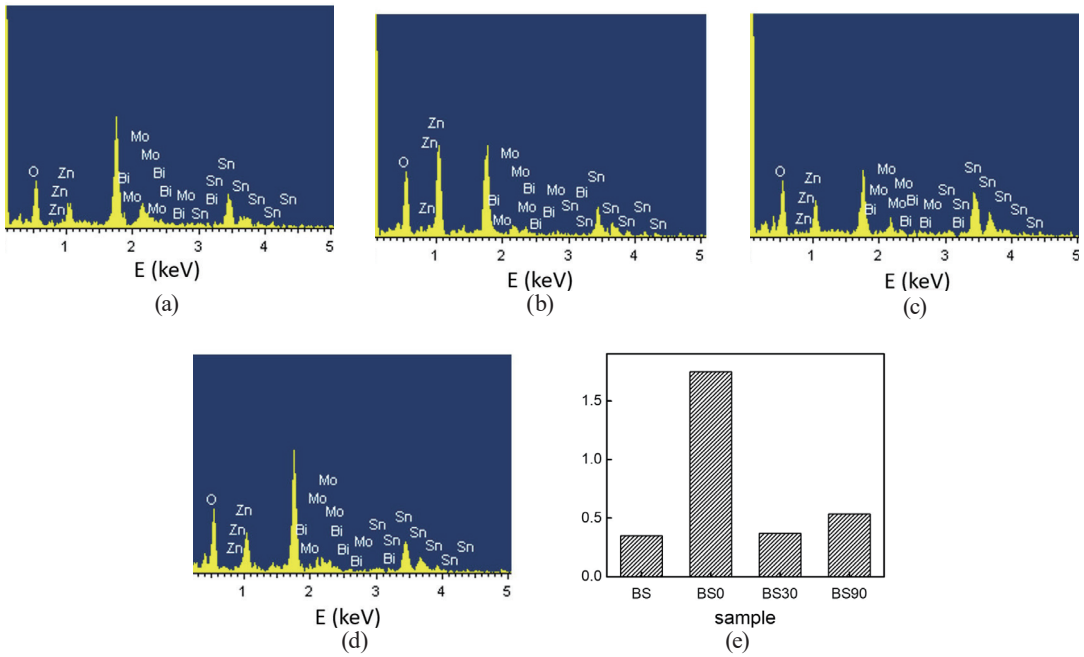

Fig. 3. (Color online) EDS spectra of (a) BS, (b) BS0, (c) BS30, and (d) BS90. (e) Corresponding Zn/Sn count ratios ($CR_{Zn/Sn}$, a.u.) of these samples.

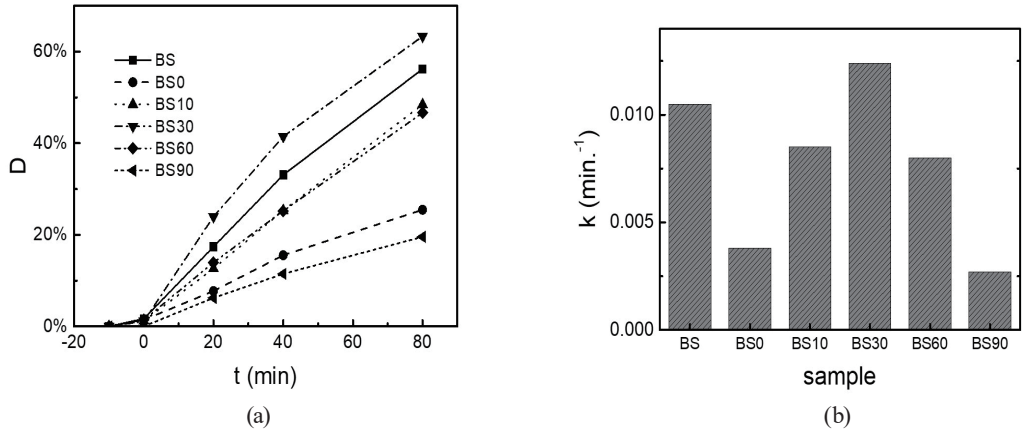

Fig. 4. (a) Degradation efficiency D of RhB for BS, BS0, BS10, BS30, BS60, and BS90 samples with illumination time t. (b) Rate constant k of each sample.

a lower k value was observed. For the samples etched by BHF, more SnOx:N and Bi_2MoO_6 were exposed and an increase in k was observed, with a relatively high value of 0.0124 min^{-1} achieved for BS30, indicating the existence of exposed SnOx:N and Bi_2MoO_6 regions suitable for the photocatalytic reaction. For samples BS60 and BS90, a decrease in k was observed. By comparing this result with the surface morphology shown in Fig. 2(e), we concluded that this was due to the lift-off of SnOx:N.

To clarify the photocatalytic mechanism and examine the effect of BHF etching, a scavenger was incorporated in the degradation of RhB under the same VL illumination condition. Benzoquinone (BQ), IPA, and ammonium oxalate (AO) were used as the scavengers to trace the states of $\bullet O_2^-$,[20] $\bullet OH$,[21] and h^+,[22] respectively. The normalized degradation efficiency for each sample was defined as

$$ND_{80} = D_{80}(\text{with scavenger}) / D_{80}(\text{no scavenger}), \tag{3}$$

where D_{80} is the degradation efficiency at an illumination time of 80 min. ND_{80} for samples BS, BS0, BS30, and BS90 is shown in Fig. 5. The choice of the scavenger affects the degradation efficiency of RhB for all samples. The band positions for Bi_2MoO_6,[23] Sn_3O_4,[18] and SnO_2[8] and the energy levels of the standard oxidation potential of $O_2/\bullet O_2^-$ and the standard reduction potential of $H_2O/\bullet OH$ are shown in Fig. 6.

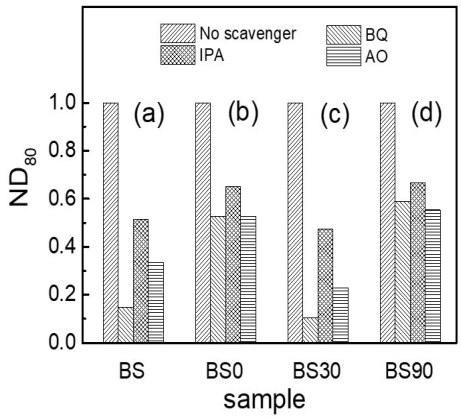

Fig. 5. Normalized degradation efficiency of RhB at time 80 min. The graph shows ND_{80} for samples BS, BS0, BS30, and BS90 with different scavengers.

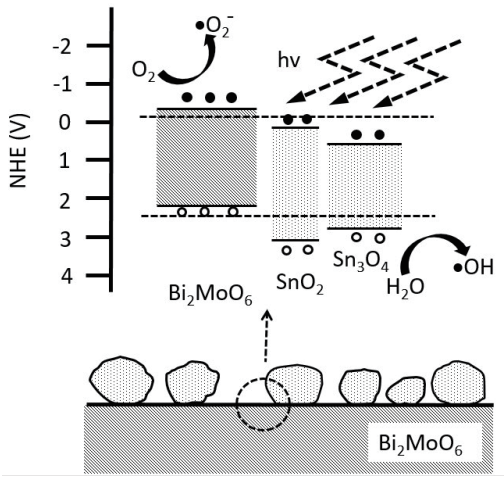

Fig. 6. Degradation mechanism of SnOx:N islands on Bi_2MoO_6.

For the Bi_2MoO_6/SnOx:N composite under VL illumination, electrons (e^-) and holes (h^+) were generated in the conduction band (CB) and valence band (VB) in the Bi_2MoO_6 and SnOx:N regions as follows:

$$Bi_2MoO_6 \,/\, SnOx{:}N + hv \rightarrow e^- + h^+. \tag{4}$$

On the Bi_2MoO_6 surface, because the CB of Bi_2MoO_6 (−0.23 eV) is higher than the standard oxidation potential of O_2/•O_2^- (−0.05 eV),[8] the electrons in Bi_2MoO_6 can react with the adsorbed O_2 to produce •O_2^-, which decomposes RhB. The degradation ability was inhibited in the case of additional BQ, as shown in Fig. 5. The formation of •O_2^- on the Bi_2MoO_6 surface can be expressed as

$$e^- + O_2 \rightarrow \bullet O_2^-. \tag{5}$$

In the band diagram shown in Fig. 6, the VB of Sn_3O_4 and SnO_2 is at 2.49 and 3.3 eV, respectively. Both quantities are below the standard reduction potential of H_2O/•OH (2.38 eV),[24] as shown in Fig. 6. Thus, the photogenerated holes on the SnOx:N surface react with H_2O to produce •OH, which decomposes RhB. The formation of •OH on the SnOx:N surface can be expressed as

$$h^+ + H_2O \rightarrow \bullet OH + H^+. \tag{6}$$

Moreover, through the reaction of the superoxide, •OH radicals can be produced as follows:[25]

$$\bullet O_2^- + \bullet O_2^- + 2H^+ \rightarrow H_2O_2 + O_2, \tag{7}$$

$$H_2O_2 + e^- \rightarrow \bullet OH + OH^-. \tag{8}$$

Thus, not all the •OH radicals originate from the photon-excited holes (h^+). This causes the difference in the degradation ability of RhB when AO and IPA are added. All scavengers inhibit the reaction shown in Fig. 5. The degradation of RhB in Bi_2MoO_6/SnOx:N is as follows:

$$e^-,\ h^+,\ \bullet O_2^-,\ \bullet OH + RhB \rightarrow \text{Degradation products}. \tag{9}$$

For sample BS, the reduced ND_{80} originating from the ability of BQ to inhibit the reaction shows that the reaction of •O_2^- radicals on the Bi_2MoO_6 surface has a photocatalytic effect. This reveals that the reactions given by Eqs. (5) and (7) may occur on the Bi_2MoO_6 beneath the SnOx:N boundary due to its grained morphology. The reduction of ND_{80} for the IPA and AO

scavengers shows that the oxidation reaction [Eq. (6)] occurred on the SnOx:N surface. The surface of sample BS0 was covered by mixed SnOx and ZnO and the less reactive surface was exposed. The ability of all scavengers was inhibited by the limited exposed surface and ND_{80} was reduced. For sample BS30, a relatively large reduction of ND_{80} was observed for BQ due to the exposure of the surface by BHF etching. From our scavenger analysis, we found that the ability of all the scavengers to inhibit the reaction was increased by the increased number of $\bullet O_2^-$ and h^+ radicals originating from the exposed Bi_2MoO_6 surface and SnOx:N surface. The difference in the inhibition abilities of BQ and IPA revealed that the surface state of SnOx:N may vary in the etching process. For sample BS90, the ability of all scavengers to inhibit the reaction was decreased. The reduction of the ability of IPA and AO was caused by the lack of SnOx:N in the etching process as shown in Fig. 2(e). ND_{80} of BQ for BS90 remained relatively high compared with those of the other samples. This reveals that the area of the exposed surface of Bi_2MoO_6 may be increased in the etching process. Carriers may recombine around the Bi_2MoO_6 surface instead of participating in the reaction in Eq. (5), thus reducing the inhibition ability of BS90 for RhB when scavenger BQ is added.

4. Conclusions

A fabrication technology based on sacrificed ZnO was studied to extend the use of the sensor material Bi_2MoO_6 by forming a novel material comprising SnOx:N islands on a Bi_2MoO_6 photocatalyst by spray pyrolysis. The morphology comprised exposed Bi_2MoO_6 and a SnOx:N surface after the etching of ZnO. The relatively high photocatalytic ability of the composite enables the exposure of SnOx:N and Bi_2MoO_6 within 30 s of etching. Scavenger analysis showed that the radicals from SnOx:N and Bi_2MoO_6 dominate the photocatalytic reaction. The exposed SnOx:N surface and Bi_2MoO_6 surface both contribute to the photocatalytic reaction. This islanding technique provides a method for controlling exposed surfaces and efficiently preparing a Bi_2MoO_6/SnOx:N composite for photocatalytic reactions.

Acknowledgments

This research was supported partly by the Ministry of Science and Technology, Taiwan. The authors thank the staff at National Sun Yat-sen University for assistance with the SEM/EDS experiments.

References

1 K. Zhenga, Y. Zhoub, L. Gua, X. Moa, G. R. Patzkeb, and G. Chena: Sens. Actuators, B **148** (2010) 240.
2 P. Tao, Y. Xu, Y. Zhou, C. Song, Y. Qiu, W. Dong, M. Zhang, and M. Shao: Mater. Res. **20** (2017) 786.
3 U. T. Nakate, P. Patil, Y. T. Nakate, S. I. Na, Y. T. Yu, and Y. B. Hahn: Appl. Surface Sci. **551** (2021) 149422.
4 J. Huang, W. Cheuk, Y. Wu, Frank S. C. Lee, and W. Ho: J. Nanomater. **2012** (2012) 753429. https://doi.org/10.1155/2012/753429
5 M. Zhang, C. Shao, J. Mu, Z. Zhang, Z. Guo, P. Zhang, and Y. Liu: CrystEngComm **14** (2012) 605.
6 H. Li, Z. Zheng, H. Jiang, D. Hu, X. Zhang, L. Xia, X. Geng, J. Lu, X. Cheng, Y. Wan, and P. Yang: Appl. Surf. Sci. **510** (2020) 145468.
7 S. Wan, Q. Zhong, M. Ou, and S. Zhang: J. Mater. Sci. **52** (2017) 11453.

8 B. Liu, X. Liu, M. Ni, C. Feng, X. Lei, C. Li, Y. Gong, L. Niu, J. Li, and L. Pan: Appl. Surf. Sci. **453** (2018) 280.
9 E. Lopez Cuellara, A. Martínez-de La Cruza, K. H. Lozano Rodrigueza, and U. Ortiz Mendeza: Catal. Today **166** (2011) 140.
10 P. Tao, Y. Xu, Y. Zhou, C. Song, Y. Qiu, W. Dong, M. Zhang, and M. Shaoa: Mater. Res. **20** (2017) 786.
11 L. Banavatu, D. S. RAO, and K. Basavaiah: Asian J. Chem. **30** (2018) 97.
12 D. J. Y. Feng, C. Y. Lai, M. C. Shih, M. Yang, W. H. Lan, M. C. Wang, and C. F. Yang: Mod. Phys. Lett. B **35** (2021) 2141007.
13 Q. Xu, L. Zhang, J. Yu, S. Wageh, A. A. Al-Ghamdi, and M. Jaroniec: Mater. Today **21** (2018) 1042.
14 Y. Xu, X. Zhang, Y. Zhang, J. Zhu, and R. Zhu: Colloid Interface Sci. Commun. **37** (2020) 100277.
15 S. N. Lou, J. Scott, A. Iwase, R. Amala, and Y. H. Ng: J. Mater. Chem. A **4** (2016) 6964. https://doi.org/10.1039/c6ta00700g
16 F. A. Alharthi, A. A. Alghamdi, N. Al-Zaqri, H. S. Alanazi, A. A. Alsyahi, A. E. Marghany, and N. Ahmad: Sci. Rep. **10** (2020) 20229. https://doi.org/10.1038/s41598-020-77426-y
17 F. Zhang, Y. Lian, M. Gu, J. Yu, and T. B. Tang: J. Phys. Chem. C **121** (2017) 16006. https//doi.org/10.1021/acs.jpcc.7b04477
18 W. Xia, H. Wang, X. Zeng, J. Han, J. Zhu, M. Zhoua, and S. Wua: CrystEngComm **16** (2014) 6841.
19 Y. Liu, P. Feng, Z. Wang, X. Jiao, and F. Akhtar: Sci. Rep. **7** (2017) 1845. https//doi.org/10.1038/s41598-017-02025-3.
20 J. Cao, B. Xu, B. Luo, H. Lin, and S. Chen: Catal. Commun. **13** (2011) 63.
21 Y. Xiang, P. Ju, Y. Wang, Y. Sun, D. Zhang, and J. Yu: Chem. Eng. J. **288** (2016) 264.
22 N. T. V. Hoan, N. N. Minh, T. T. K. Nh, N. V. Thang, V. A. Tuan, V. T. Nguyen, N. M. Thanh, N. V. Hung, and D. Q. Khieu: J. Nanomater. **2020** (2020) 4350125. https://doi.org/10.1155/2020/4350125
23 Y. Peng, Y. Zhang, F. Tian, J. Zhang, and J. Yu: Crit. Rev. Solid State Mater. Sci. **42** (2017) 347. https://doi.org/10.1080/10408436.2016.1200009
24 S. P. Kim, M. Y. Choi, and H. C. Choi: Mater. Res. Bull. **74** (2016) 85.
25 A. Fujishima and X. Zhang: C. R. Chim. **9** (2006) 750. https://doi.org/10.1016/j.crci.2005.02.055